Assessment of rotational stiffness in HSS-UHPC composite cellular beams under hogging moment

Flávia Gimenez Berti[1], Alexandre Rossi[2], Vinicius Moura de Oliveira[3], Carlos Humberto Martins[4]

[1]*Departament. of Civil Engineer, State University of Maringá*
5790 Colombo Avenue – Zona 7, 87020-900, Paraná, Brazil
[1]*pg405387@uem.br,* [2]*arossi@uem.br,* [3]*engenheiro.viniciusmoura@gmail.com,* [4]*chmartins@uem.br*

Abstract. Composite steel-concrete cellular beams are widely used in continuous systems, where the verification of the hogging moment region is critical to prevent lateral-distortional buckling (LDB). Design codes recommend estimating the elastic critical moment using the inverted U-frame mechanism, which considers the rotational stiffness of each component to evaluate the overall stiffness of the system. However, current methodologies do not fully reflect the range of geometries and material strengths found in modern composite construction. This study presents a sensitivity analysis to investigate the main parameters influencing the rotational stiffness of composite cellular beams. In addition to conventional materials, models using high-strength steel (HSS) and ultra-high-performance concrete (UHPC) were also analyzed to explore the influence of advanced materials on stiffness behavior. Finite element models were developed in ABAQUS and validated against experimental data from literature. Results show that the flexibility of the steel profile governs approximately 90% of the total deformability of the mechanism, significantly exceeding the contributions of the slab and shear connection. Therefore, parameters related to the steel profile, especially web thickness and opening diameter, were identified as the most influential in stiffness behavior.

Keywords: rotational stiffness, lateral distortional buckling, composite beams.

1 Introduction

Continuous steel-concrete composite beams, commonly used in bridges, floors, and industrial buildings, are formed by the interaction between a concrete slab and a steel profile. In hogging moment regions, compressive forces in the steel section and tensile stresses in the slab may lead to Lateral Distortional Buckling (LDB). This instability is assessed using the Elastic Critical Moment (M_{cr}), calculated through the Inverted U-frame mechanism (Fig. 1) adopted by design standards such as Eurocode 4 [1], which simulates the system with a rotational spring (k_r) acting on the top flange to represent the lateral and torsional restraints provided by the slab, web, and connectors.

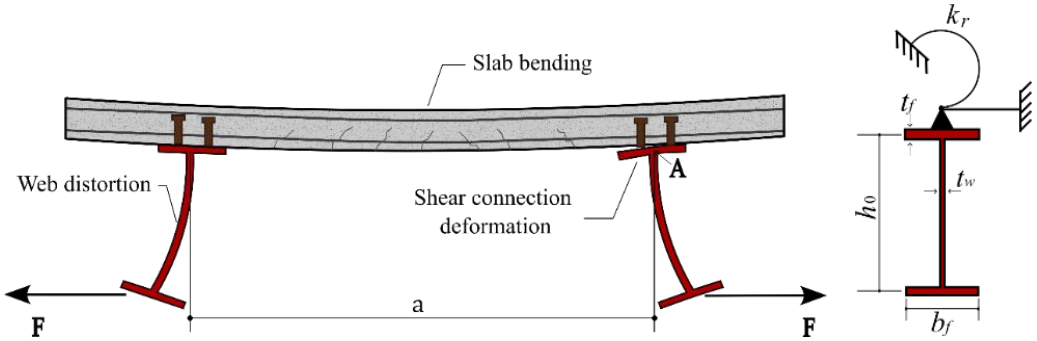

Figure 1. Inverted U-frame mechanism and k_r representation

The rotational stiffness per unit length (k_r) is a key parameter in the prediction of M_{cr} and is obtained by the series combination of the slab bending stiffness (k_1), web distortion stiffness (k_2), and connector stiffness (k_3), the latter often being neglected due to its relatively high magnitude. These relationships are expressed in eqs. (1)–(3), originally developed for I-section beams without web openings. Dietrich et al. [2] numerically investigated the components of k_r and confirmed the relevance of eq. (3) for this type of I-section, but proposed a correction factor for eq. (2). Rossi et al. [3], comparing M_{cr} analytical values to numerical simulations, showed that discrepancies may still arise due to simplifications in the analytical approach, even for solid web profiles.

$$k_r = \left(\frac{1}{k_1} + \frac{1}{k_2} + \frac{1}{k_3}\right)^{-1} \quad (1)$$

$$k_1 = \frac{\alpha (EI)_2}{a} \quad (2)$$

$$k_2 = \frac{E_a {t_w}^3}{4(1 - {\nu_a}^2) h_0} \quad (3)$$

For beams with web openings, adjustments to the web stiffness term have been proposed, such as in the works of Silva et al. [4] for castellated profiles and Müller et al. [5] for cellular profiles. However, few studies investigate the global rotational stiffness (k_r) directly in composite cellular beams, particularly when incorporating high-performance materials like UHPC and HSS, despite their growing application and potential structural benefits. To address this research gap, the present study conducts validated numerical simulations of the Inverted U-frame model in Abaqus, aiming to assess the influence of advanced material combinations and geometric parameters on k_r.

2 Definition and calibration of the numerical model

Before conducting the parametric analyses, two numerical models were validated: one based on the experimental study by Calenzani et al. [6], which reproduces the Inverted U-frame mechanism, and the other based on Qi et al. [7], aimed at accurately modeling UHPC behavior. The boundary conditions adopted in each validation are shown in Fig. 2. To define the material behavior, conventional steel was modeled using the Earl's model [8,9], and reinforcement bars with a linear hardening model. Concrete behavior followed Carreira and Chu [10] for conventional concrete and Krahl et al. [11] for UHPC in compression. The UHPC tensile behavior was modeled using the approach by Li and Leung [12], considering crack opening and fiber contribution. Concrete Damage Plasticity (CDP) was adopted for both concretes, using parameters from Oliveira et al. [13], Rossi et al. [14], and Sousa et al. [15].

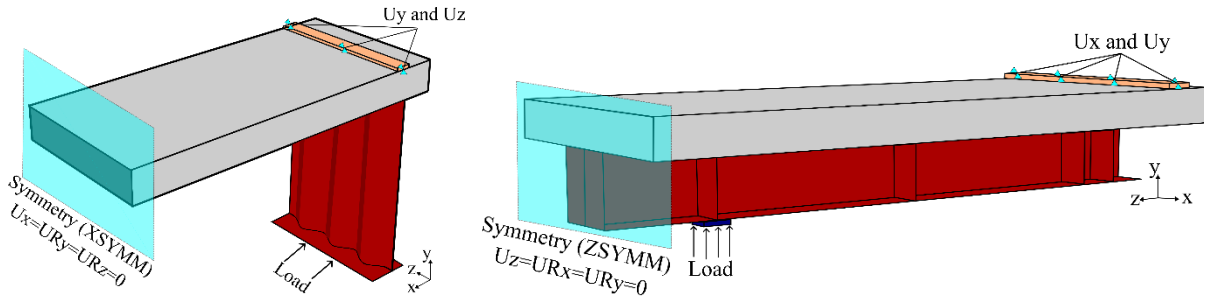

(a) Calenzani et al. [6] (b) Qi et al. [7]

Figure 2. Boundary conditions regarding the specimens.

For both validations, steel profiles were modeled with shell elements (S4R), while the concrete slab, actuator, and shear connectors were modeled with solid elements (C3D8R). Reinforcement bars were defined with T3D2 elements using the embedded region technique. Contact interactions were simulated using surface-to-surface

contact with hard contact in the normal direction and penalty formulation in the tangential direction, with a friction coefficient of 0.4. Welded connections were modeled using Tie constraints. The symmetry command was applied, and displacement control was used to simulate loading. In the U-frame validation, no imperfections or residual stresses were applied, as the focus was on composite rotation. In the UHPC based model, residual stresses were introduced using the ECCS (1984) pattern, and initial geometric imperfections were applied based on the first buckling mode using an amplitude of d/100, as suggested in some studies [16].

The validation results demonstrated good agreement with experimental data, as shown in Fig. 3. In the U-frame model, the rotational stiffness (k_r) was obtained from the initial slope of moment–rotation curves, with rotations extracted from two sections at the bottom flange and averaged. The numerical results closely matched the experimental ones, especially for the prototype U1-P (Fig. 3a). In the UHPC model (Fig. 3c), the numerical ultimate load differed by only 0.46% from the experimental value, confirming the model's reliability for use in parametric studies.

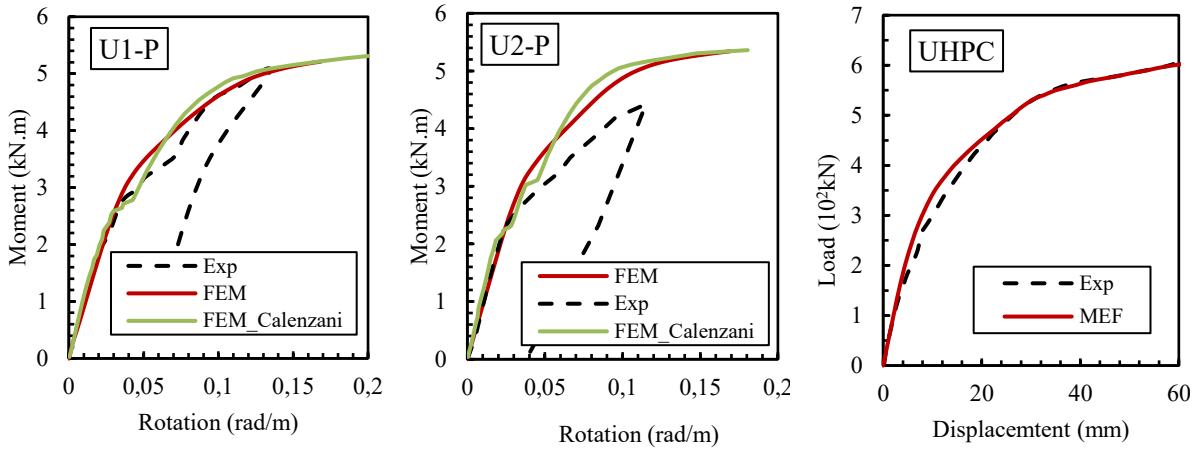

Figure 3. Numerical validation model.

3 Parametric study

A sensitivity study was conducted to evaluate the influence of key geometric and material parameters on the equivalent rotational stiffness (k_r) of composite beams. The parameters investigated include steel section height (d), opening diameter (a_0), spacing between opening centroids (p), slab thickness (h_s), web thickness (t_w) and material properties. Two concrete types were considered, C50 and UHPC, as well as two steel grades, high-strength steel (S690) and conventional S355. This analysis was performed using the numerical model based on the Inverted U-frame mechanism previously validated by Calenzani et al. [6]. The parent section adopted to this study was only UB 254x102x25, which parameters are presented in Tab. 1. Constitutive models adopted were those previously calibrated for S355, C50 and UHPC, and the Yun and Gardner [17] model for high-strength steel.

Table 1. Parameters of Universal Beam UB 254 x 102 x 25

Profile	d_0 (mm)	b_f (mm)	t_w (mm)	t_f (mm)
UB 254x102x25	257.2	101.9	6	8.4

3.1 Procedure for stiffness determination

The rotational stiffness of each component of the composite beam was determined through the analysis of moment-rotation curves. The applied moment was calculated as the product of the reaction force and the vertical distance between the centroids of the top and bottom flanges of the steel profile. To isolate the contribution of each component, rotations and vertical displacements were collected at three distinct sections along the beam: aligned with the shear connector; between two connectors and within the web-post region (Double-T region).

The rotation collected at the bottom flange of the steel profile (θ_R) corresponds to the total rotation of the

mechanism. Meanwhile, the rotation of the top flange (θ) was used to estimate the relative flexibility of the connection (θ_3). Additionally, vertical displacements were extracted at points positioned immediately internal (U_{y1}) and external (U_{y2}) to the U-frame mechanism to estimate the flexibility of the slab (θ_1), particularly in cracked regions. Equations. (4)-(6) define the procedures used to calculate the flexibilities of the slab, web (θ_2) and the shear connection, respectively, where b represents the distance between the reference points.

$$\theta_1 = \frac{|U_{y1} - U_{y2}|}{b} \qquad (4)$$

$$\theta_3 = |\theta - \theta_1| \qquad (5)$$

$$\theta_2 = |\theta_R - \theta| \qquad (6)$$

To ensure consistency across all models, the stiffness values were normalized by the actual profile length (L), which varied according to the opening diameter defined in each parametric configuration. The values of k_r, k_2 and k_3 were obtained through linear regression applied to the initial elastic portion of the moment-rotation curves, indicated by red marks in Fig. 4a. For the cracked slab stiffness (k_1), a standardized procedure was adopted: a line parallel to the initial elastic branch, indicated by green line in Fig. 4b, was offset by $\Delta\theta$ = 0.001 rad/m, and its intersection with the curve defined the starting point for regression. From this point forward, a minimum of 20 and a maximum of 100 data points were considered to fit a straight line, with a coefficient of determination (R^2) equal to or greater than 0.99, thereby ensuring that k_1 accurately represented the post-cracking behavior of the slab. All stiffness values were calculated as the tangent slope of the corresponding fitted lines and expressed in kN·m/rad·m.

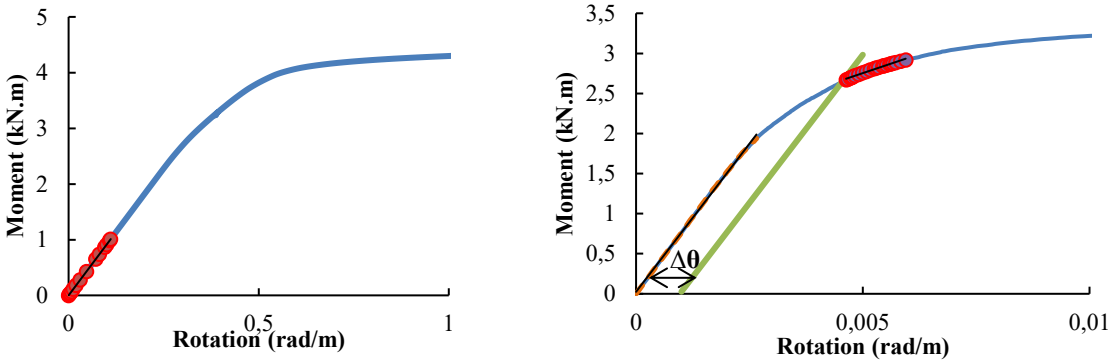

(a) Procedure for obtain k_r, k_2 and k_3 (b) Procedure for obtain k_1

Figure 4. Procedure for determine rotational stiffness of elements.

3.2 Influence of geometric parameters or the steel profile

The influence of geometric parameters related to the steel profile was investigated through a sensitivity analysis considering variations in section height, opening diameter, web thickness, and web-post width. The section height was varied using expansion ratios of $1.4d_0$ and $1.6d_0$, where d_0 is the height of the parent section (UB 254x102x25). The diameter of the circular web openings was varied using ratios of $0.9d_0$, $1.0d_0$, and $1.2d_0$. The distance between the centroids of adjacent openings (p), was studied using two ratios: $1.2a_0$ and $1.5a_0$. Regarding web thickness, two configurations were analyzed: the original value (6 mm) and double that thickness.

An analysis of the effect of section height showed that increasing the height of the steel profile leads to a reduction in the equivalent rotational stiffness of the composite alveolar beam. Similarly, regarding the distance between the centroids of adjacent openings, it was observed that shorter distances result in lower rotational stiffness. The reference configuration for this analysis consists of a UB 254x102x25 profile with height $1.4d_0$ (360.08 mm), 80 mm slab thickness, C50–S690 materials and p=$1.5a_0$. These results are presented in Fig. 5a, where the red markers correspond to the profile with a height of $1.6d_0$ (411.52 mm), and triangular markers indicate variations in the web-post spacing, for the three opening diameters evaluated. Among the parameters investigated, the web thickness had the most significant influence on the rotational stiffness. The increase in web

thickness also led to a reduction in the rotation of the bottom flange, as the web becomes stiffer and more resistant to distortion. This behavior results in higher rotational stiffness, as observed in the analysis and as was expected based on structural mechanics principles. These results are illustrated in Figure 5b.

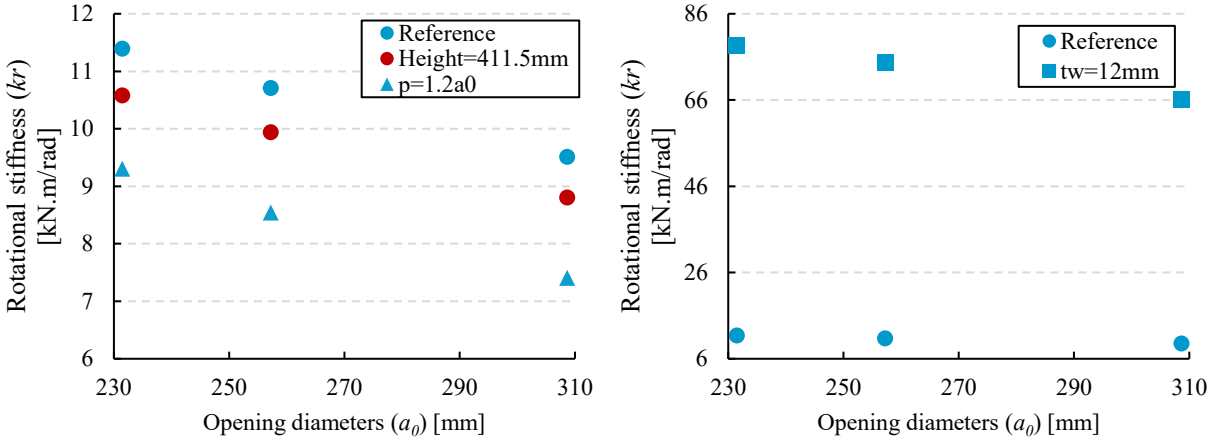

Figure 5. Influence of (a) height, opening diameter, spacing between opening centroids and (b) web thickness.

3.3 Influence of slab thickeness

The effect of slab thickness on the rotational stiffness (k_r) is not evident, like showed Fig. 6a. Qualitative observations of the models indicate that thicker slabs tend to exhibit reduced cracking, especially near the interface with the steel section. This is illustrated in Fig. 6b and 6c, which shows the cracking patterns observed in models with different slab thicknesses, extracted at the same load increment, allowing a consistent comparison.

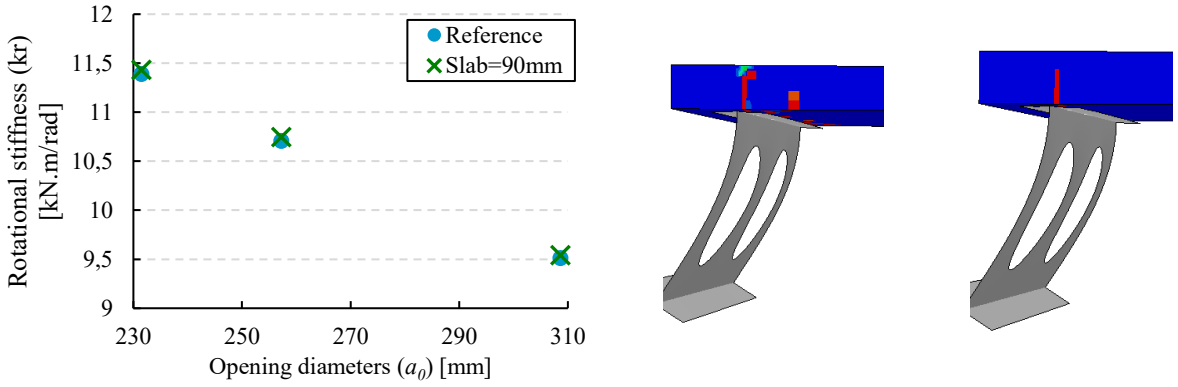

Figure 6. Influence of (a) slab thickness and (b) cracking pattern in slab 80 mm and (c) 90 mm.

This behavior suggests that the influence of slab thickness on rotational stiffness is not isolated, but rather strongly dependent on the interaction with other geometric parameters, especially those related to the steel profile, discussed in Section 3.2. This is particularly relevant for composite cellular beams with web openings, where the steel profile plays a dominant structural role in the Inverted U-frame mechanism. The cracking behavior observations highlight that slab thickness contributes to the damage control of the composite beam.

3.4 Influence of material properties

Four combinations of concrete and steel were analyzed to evaluate the influence of material properties on the rotational stiffness (k_r): C50–S355, C50–S690, UHPC–S355, and UHPC–S690. Among these parameters, the influence of steel strength was notably more significant. This can be explained by the fact that the rotational stiffness of composite cellular beams is predominantly governed by the rotational stiffness of the steel web. As

shown in Fig. 7a, an increase in steel grade from S355 to S690 leads to a clear increase in k_r, regardless of the concrete used. It is also observed that the rotational stiffness for the UHPC–S355 combination is lower than that obtained for C50–S355, probably due to the load level applied to the system. Since UHPC exhibits higher compressive strength, the imposed loading in the numerical model is greater for this case. The combination of higher applied loading with a conventional steel profile (S355) leads not to performance gains, but rather to a reduction in stiffness or an increase in flexibility.

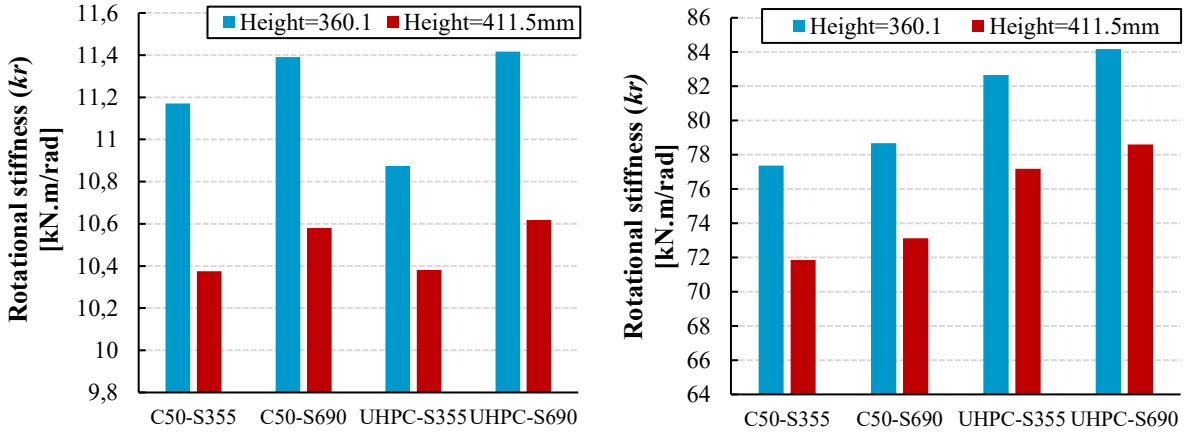

(a) Diameter 231.48 mm and Slab 80 mm (b) Diameter 231.48 mm and Slab 80 mm

Figure 7. Influence of material proprieties in profiles with (a) t_w= 6 mm and (b) t_w= 12 mm.

To further illustrate the importance of the steel profile in determining the rotational stiffness, an additional analysis was performed using the same cellular beams with increased web thickness. These beams were reanalyzed with the same material variations to assess whether the influence of concrete strength becomes more pronounced in profiles with stiffer webs. Fig. 7b showed that the role of the slab in these beams become clearer, allowing the difference between C50 and UHPC to be better observed.

3.5 Contribution of each element

To demonstrate and quantify the influence of each element of composite cellular beam in rotational stiffness value, Tab. 2 presented the ratios of slab, web and connectors flexibility (θ_1, θ_2 e θ_3) and total flexibility (θ_r). These results were collected for slab thickness of 80 mm, p=1.5a_0 and t_w= 6 mm, with the remaining parameters specified in the table. Since flexibility is the inverse of stiffness, it can be observed that the web is significantly more flexible than the other components, primarily due to the presence of web openings, accounting for approximately 90% of the total flexibility.

Table 2. Influence of each element in rotational stiffness

Concrete	Steel	h (mm)	a_0 (mm)	*k1*	*k2*	*k3*	θ1/θr	θ2/θr	θ3/θr
C50	S355	360.08	231.48	244.33	11.47	295.75	4.3%	92.1%	3.6%
C50	S690	360.08	231.48	244.66	11.70	296.41	4.4%	92.0%	3.6%
C50	S355	360.08	257.2	479.07	10.80	271.11	2.1%	94.1%	3.8%
C50	S690	360.08	257.2	289.41	11.02	272.81	3.5%	92.7%	3.7%
UHPC	S355	360.08	231.48	42.42	11.13	349.74	20.3%	77.3%	2.5%
UHPC	S690	360.08	231.48	183.40	11.70	350.43	5.8%	91.1%	3.0%
UHPC	S355	360.08	257.2	108.45	10.51	314.74	8.6%	88.5%	3.0%
UHPC	S690	360.08	257.2	132.75	11.02	321.55	7.4%	89.5%	3.1%
C50	S355	411.52	231.48	207.27	10.65	283.52	4.7%	91.8%	3.5%

C50	S690	411.52	231.48	255.22	10.87	285.00	3.9%	92.5%	3.5%
C50	S355	411.52	257.2	383.62	10.01	265.90	2.5%	94.0%	3.5%
C50	S690	411.52	257.2	345.28	10.21	267.66	2.8%	93.7%	3.6%
UHPC	S355	411.52	231.48	94.63	10.63	333.89	9.8%	87.4%	2.8%
UHPC	S690	411.52	231.48	260.95	10.87	341.17	3.9%	93.2%	3.0%
UHPC	S355	411.52	257.2	95.05	10.00	309.36	9.2%	87.9%	2.8%
UHPC	S690	411.52	257.2	175.94	10.21	317.05	5.3%	91.7%	3.0%

4 Conclusions

Based on the results and discussions regarding the influence of various parameters on the rotational stiffness of steel-concrete composite cellular beams, it can be concluded that parameters related to the steel profile have the greatest impact on the determination of k_r. Increasing the web thickness enhances the resistance of web and, consequently, leads to higher rotational stiffness and lower flexibility under loading in the Inverted U-frame mechanism. Additionally, the diameter of the web openings exhibited a significant influence on k_r, with larger openings generally reducing stiffness. Regarding material properties, it was observed that once the influence of the steel profile decreases, as in cases where the web thickness is relatively high (t_w= 12 mm), the concrete slab material begins to play a more prominent role in defining the overall rotational stiffness. Furthermore, increasing the steel yield strength also contributes to greater profile stiffness and, consequently, higher k_r values.

Acknowledgements. The authors would like to thank the Conselho Nacional de Desenvolvimento Científico e Tecnológico (CNPq) for the support in the execution of the research project and for providing access for the computational resources of Amazon Web Services Elastic Compute Cloud Platform – Amazon AWS-EC2. Grant number #421785/2022-5, 408498/2022-6 and 301023/2025-5.

References

[1] EN 1994-1-1: Eurocode 4- Design of composite steel and concrete structures - Part 1-1: General rules and rules for buildings, 2024.

[2] M.Z. Dietrich, A.F.G. Calenzani, R.H. Fakury, Analysis of rotational stiffness of steel-concrete composite beams for lateral-torsional buckling, Eng Struct 198 (2019). https://doi.org/10.1016/j.engstruct.2019.109554.

[3] A. Rossi, F.P.V. Ferreira, C.H. Martins, E.C. Mesacasa Júnior, Assessment of lateral distortional buckling resistance in welded I-beams, J Constr Steel Res 166 (2020). https://doi.org/10.1016/j.jcsr.2019.105924.

[4] C.C. Silva, R.B. Caldas, R.H. Fakury, H. Carvalho, J.V.F. Dias, Web rotational stiffness of continuous steel-concrete composite castellated beams, Frattura Ed Integrita Strutturale 13 (2019) 264–275. https://doi.org/10.3221/IGF-ESIS.50.22.

[5] Müller et al., Large web openings for service integration in composite floors, 2006. http://ec.europa.eu/research/rtdinfo/index_en.html.

[6] A.F.G. Calenzani, R.H. Fakury, F.A. De Paula, F.C. Rodrigues, G. Queiroz, R.J. Pimenta, Rotational stiffness of continuous composite beams with sinusoidal-web profiles for lateral-torsional buckling, J Constr Steel Res 79 (2012) 22–33. https://doi.org/10.1016/j.jcsr.2012.07.015.

[7] J. Qi, Z. Cheng, J. Wang, Y. Tang, Flexural behavior of steel-UHPFRC composite beams under negative moment, Structures 24 (2020) 640–649. https://doi.org/10.1016/j.istruc.2020.01.022.

[8] C.J. Earls, Effects of material property stratification and residual stresses on single angle flexural ductility, 1999. www.elsevier.com/locate/jcsr.

[9] C.J. Earls, On the inelastic failure of high strength steel I-shaped beams, 1999.

[10] D.J. Carreira, K.-H. Chu, Stress-Strain Relationship for Plain Concrete in Compression, ACI Journal (1985) 797–804.

[11] P.A. Krahl, G. de Miranda Saleme Gidrão, R. Carrazedo, Compressive behavior of UHPFRC under quasi-static and seismic strain rates considering the effect of fiber content, Constr Build Mater 188 (2018) 633–644. https://doi.org/10.1016/j.conbuildmat.2018.08.121.

[12] V.C. Li, C.K.Y. Leung, STEADY-STATE AND MULTIPLE CRACKING OF SHORT RANDOM FIBER COMPOSITES, J. Eng. Mech. 118 (1992) 2246–2264.

[13] V.M. de Oliveira, A. Rossi, F.P.V. Ferreira, C.H. Martins, Stability behavior of steel–concrete composite cellular beams subjected to hogging moment, Thin-Walled Structures 173 (2022). https://doi.org/10.1016/j.tws.2022.108987.

[14] A. Rossi, A.S.C. de Souza, R.S. Nicoletti, C.H. Martins, Stability behavior of Steel–concrete Composite Beams subjected to hogging moment, Thin-Walled Structures 167 (2021). https://doi.org/10.1016/j.tws.2021.108193.

[15] A.M.D. de Sousa, E.O.L. Lantsoght, A.S. Genikomsou, P.A. Krahl, M.K. El Debs, Behavior and punching capacity of flat slabs with the rational use of UHPFRC: NLFEA and analytical predictions, Eng Struct 244 (2021). https://doi.org/10.1016/j.engstruct.2021.112774.

[16] V.M. de Oliveira, L.M.S. Prates, A. Rossi, J.P. Martins, L.A.P. Simões da Silva, C.H. Martins, Comparative analysis of geometric imperfections and residual stresses on the global stability behavior of cantilever composite alveolar beams, Structures 65 (2024). https://doi.org/10.1016/j.istruc.2024.106634.

[17] X. Yun, L. Gardner, Stress-strain curves for hot-rolled steels, J Constr Steel Res 133 (2017) 36–46. https://doi.org/10.1016/j.jcsr.2017.01.024.